Climate Dynamics
https://doi.org/10.1007/s00382-020-05243-0

Joint impact of North Pacific Victoria mode and South Pacific Quadrapole mode on Pacific ITCZ summer precipitation

Xumin Li[1] · Wenjun Zhang[1] · Ruiqiang Ding[2] · Liang Shi[3]

Received: 28 October 2019 / Accepted: 10 April 2020

Abstract
This study investigates the joint impact of the boreal late winter–early spring North Pacific Victoria mode (VM) and South Pacific Quadrapole (SPQ) mode on the following summer Pacific Intertropical Convergence Zone (ITCZ) precipitation. Here, both observational data and historical simulations from the Coupled Model Intercomparison Project Phase 5 (CMIP5) models show that the precipitation anomalies are enhanced when the VM and the SPQ are in phase but are weakened when they are out of phase. The strength of the anomalous vertical velocity (ω) and outgoing longwave radiation also tend to be stronger (weaker) in same-sign (opposite-sign) events. One possible reason for this is that when the VM and the SPQ are in (out of) phase, westerly anomalies over the western–central tropical Pacific are greatly increased (reduced) due to the interactions between preceding North and South Pacific sea surface temperature anomalies, thereby enhancing (reducing) convective upward motion over the western and central Pacific. In addition, an empirical linear regression model is also developed to forecast Pacific ITCZ summer precipitation based on both the late winter–early spring VM and SPQ indices. The combination of the two precursors in North and South Pacific show higher prediction skills than the single VM or SPQ model, which means it is necessary to consider their joint impact when we focus on the Pacific ITCZ precipitation.

Keywords Intertropical Convergence Zone · Precipitation · Victoria mode · South Pacific Quadrapole mode

1 Introduction

The Intertropical Convergence Zone (ITCZ) is a region of low pressure within the tropical belt and is characterized by rising air, cloudiness, and deep convective precipitation (Mechem 2013). Therefore, due to its strong and sustained convective activity, the ITCZ plays a critical role in the atmospheric energy budget and global climate variability (Castelli et al. 2018). For example, the ITCZ forms the ascending branch of the Hadley cells of the atmosphere and helps to compensate for the uneven solar radiation. When the northward extent of the ITCZ and its precipitation intensity decrease in boreal summer, the summer monsoon rains weaken in parts of South Asia (Clement et al. 2004; Cheng et al. 2012).

The mechanisms driving the location of the ITCZ and its precipitation intensity are significant issues that remain unresolved in climate dynamics, so it is of great importance to identify climate precursors that are closely related to the ITCZ. Previous studies have linked the location and intensity of the ITCZ to local tropical influences on interannual timescales (e.g., Chiang et al. 2002; Gu et al. 2005; Chou and Lo 2007; Zhan et al. 2011), such as El Niño-Southern Oscillation (ENSO; Bjerknes 1969; Mcphaden et al. 2006). The latitudinal average position of the ITCZ was closely related to the transport of energy across the equatorial atmosphere from observations (e.g., Donohoe et al. 2013, 2014; Adam et al. 2016) and climate models (e.g., Kang et al. 2008, 2009; Donohoe et al. 2013, 2014). In addition, Dai et al. (2000) and Liu et al. (2012) found that the western and central Pacific ITCZ shifted southward by about 2° from typical La Niña to El Niño conditions, and shifted southward by about

✉ Ruiqiang Ding
drq@mail.iap.ac.cn

[1] CIC-FEMD/ILCEC, Key Laboratory of Meteorological Disaster of Ministry of Education, School of Atmospheric Sciences, Nanjing University of Information Science and Technology, Nanjing 210044, China

[2] State Key Laboratory of Earth Surface Processes and Resource Ecology, Beijing Normal University, Beijing 100875, China

[3] School of Science, Lanzhou University of Technology, Lanzhou 730050, China

Published online: 18 April 2020

5° when the El Niño events was strong. Bain et al. (2011) showed that the ITCZ position and the intensity of related phenomena are associated with the magnitude of ENSO. The mean annual ITCZ locations expand in El Niño events and shrink in La Niña events. Nevertheless, after removing ENSO signal, there remains considerable unexplained variability from year to year. This suggests that there exist other factors, independent of the strongest interannual climate fluctuation on earth (ENSO), that affect the location and magnitude of the ITCZ.

In addition to the impacts from the tropics, many paleoclimatic and modeling studies have shown that the position of the ITCZ is affected by perturbations of thermal forcing in the extratropics, including the thermohaline circulation in the Atlantic (Zhang and Delworth 2005) and high-latitude land ice, sea ice, and ocean heat transport (Chiang et al. 2003; Chiang and Bitz 2005). Pausata and Camargo (2019) demonstrated that volcanic eruptions can also shift the ITCZ southward or northward due to the strong asymmetrical hemispheric cooling, which is consistent with the classical theory (antisymmetric interhemispheric heating) proposed by Broccoli et al. (2006). In addition, many scholars have focused on the extratropical Pacific influence on ITCZ precipitation. For example, the Victoria mode (VM) (Bond et al. 2003), second dominant mode in the North Pacific, is shown to be an important precursor for the following summer ITCZ precipitation (Ding et al. 2015a). That study pointed out that after strong positive VM events, there are usually positive (negative) precipitation anomalies over the tropical central–eastern (western and eastern) Pacific ITCZ region. Qin et al. (2018) found that the South Pacific Quadrapole (SPQ) mode, a SST anomaly pattern poleward of 20°S (Ding et al. 2014), can have a substantial impact on precipitation over the South Pacific Convergence Zone (SPCZ; Trenberth 1976) and ITCZ via the wind-evaporation-SST (WES) mechanism (Xie and Philander 1994).

Since the North and South Pacific extratropical SST both have close relationship with subsequent Pacific ITCZ summer precipitation, one may wonder whether the VM influence interferes with that of the SPQ. Previous researches have primarily focused on the individual influence of the North and South Pacific SST on Pacific ITCZ summer precipitation, with little discussion of their joint role. Thus, here we investigate the joint impact of the North and South Pacific SST anomalies on subsequent Pacific ITCZ summer precipitation.

In Sect. 2, the observations, model datasets, and index definitions used in this study are described. Section 3 examines the joint connections between Pacific ITCZ precipitation anomalies and antecedent VM and SPQ from observations. In Sect. 4, the mechanism underlying the joint impact of VM and SPQ on precipitation over the tropical Pacific is analyzed. Section 5 uses output of models to verify our findings. Then, in Sect. 6 several prediction models are developed to predict the ITCZ summer precipitation. Finally, discussion and conclusion are presented.

2 Data and methods

2.1 Observational datasets

The SST data used in this study are from the Hadley Centre Sea Ice dataset (HadISST) on a $1° \times 1°$ horizontal grid (Rayner et al. 2003). The monthly precipitation data (mm day^{-1}) utilized are from the Climate Prediction Center Merged Analysis of Precipitation (CMAP; Xie and Arkin 1997). To verify the CMAP results, the Global Precipitation Climatology Project (GPCP; Huffman et al. 1997; Adler et al. 2003) dataset is also used. Both datasets of precipitation are at a resolution of $2.5° \times 2.5°$. In addition, *u*-wind, *v*-wind, and vertical velocity (ω) are obtained from the National Centers for Environmental Prediction–National Center for Atmospheric Research (NCEP–NCAR) reanalysis version I on a $2.5° \times 2.5°$ grid (Kalnay et al. 1996). To characterize tropical convective activity, we also use the outgoing longwave radiation (OLR) data from the National Oceanic and Atmospheric Administration (NOAA; Liebmann and Smith 1996). All data applied in the analysis are for the period 1979–2017, because the datasets mentioned above are all available for this period. The long-term linear trends and seasonal cycles of all variables are removed prior to analysis. Late winter–early spring and summer are defined as February–April (FMA) and June–August (JJA), respectively, and correspond to boreal late winter–early spring and summer.

2.2 Model datasets

To evaluate whether the joint relationship between boreal summer Pacific ITCZ precipitation and antecedent VM and SPQ can be reproduced in current coupled models, we use monthly output from historical experiments from 25 coupled atmosphere–ocean models that participated in CMIP5 (Coupled Model Intercomparison Project, Phase 5). The variables we analyzed here are monthly SST, precipitation, and horizontal winds from 1905 to 2004. What's more, for ease of comparison and ensemble mean calculations, we convert all variables from the CMIP5 output into a horizontal resolution of $2.5° \times 2.5°$. The significance of correlation and composite values from both observed and modeled dataset is tested by a two-tailed Student's *t* test (Li et al. 2012, 2013).

2.3 Definitions of indices

According to Bond et al. (2003), the VM is defined as the second empirical orthogonal function mode (EOF2)

of monthly SST anomalies over the North Pacific (120°E–150°W, 20°–60°N) for the period 1979–2017 (Fig. 1a). The prominent feature of the VM is a tilted SST anomaly dipole structure oriented in the northeast–southwest direction over the North Pacific, characterized by a band of positive SST anomalies extending from the Sea of Okhotsk to northeastern North Pacific and a band of negative SST anomalies extending from the central North Pacific to the western North Pacific (Fig. 1a). Naturally, the VM index (VMI) is the principal component (PC2) associated with the EOF2 (Ding et al. 2015a).

The SPQ is triggered by SLP variability over the South Pacific with a zonal wave number-3 structure, which resembles the PSA (Pacific-South American; Mo and Higgins 1998) pattern. Following Ding et al. (2014), the SPQ index (SPQI) is obtained by calculating the difference between the sum of normalized SST anomalies over the areas B and D and the sum of normalized SST anomalies over the areas A and C (Fig. 1b). The most obvious feature of the SPQ pattern is a quadrapole-like SST anomaly structure over the South Pacific, with centers over the Tasman Sea off the southeast coast of Australia, the Ross Sea, the Bellingshausen Sea, and the west coast of South America (Fig. 1b). The correlation coefficients between simultaneous SST anomalies and the SPQI prominent anomalies coincide with the locations of the four boxes.

Figure 1c presents the monthly time series of the VMI and SPQI. Their correlation coefficient is not significant at the 95% confidence level (R = 0.26), which indicates that the two series are relatively independent of each other. Previous studies reported that both the VM and SPQ have the maximum variance around boreal late winter–early spring (Ding et al. 2014, 2015b). Thus, our research uses the three-month averaged FMA VMI and SPQI. A year in which the FMA VMI (SPQI) > 0 is defined as a VM+ (SPQ+) event, and a VM− (SPQ−) event is a year in which the FMA VMI (SPQI) < 0.

3 Joint relationship of the VM and SPQ with the Pacific ITCZ precipitation

Figure 2a shows the spatial map of correlations between the FMA VMI and the JJA precipitation anomalies. There are positive and strong correlations over the central tropical Pacific, whereas significant negative correlations over the western tropical Pacific. These inhomogeneous spatial patterns are in agreement with the results of Ding et al. (2015a). Similarly, Fig. 2b shows a spatial map of correlations between the FMA SPQI and the following JJA precipitation anomalies, in which there are also two significantly correlated regions. Over the western Pacific (WP), there are strong negative correlations, whereas over the central Pacific (CP) there are significant positive correlations. The climatological mean precipitation during JJA is indicated with green contours in Fig. 2. Similar patterns are obtained using the GPCP dataset (not shown). The above results indicate that both the VM and SPQ have positive correlations with central Pacific ITCZ summer precipitation and negative correlations with western Pacific ITCZ summer precipitation. Similar

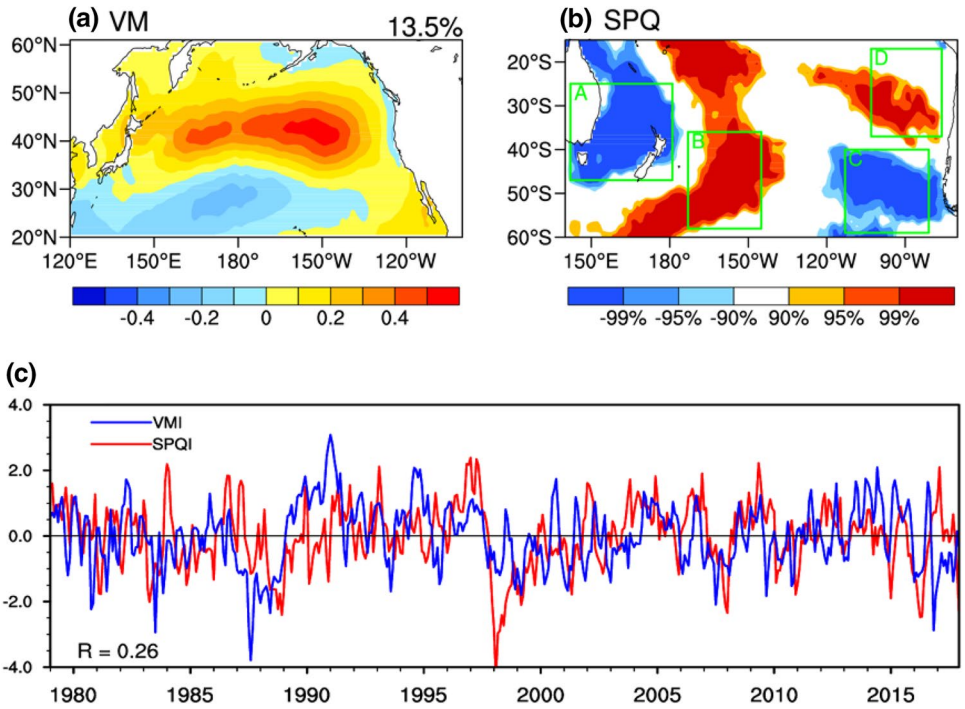

Fig. 1 **a** Spatial pattern of the EOF2 mode of North Pacific (120°E–100°W, 20°–61°N) monthly SST anomalies for the period 1979–2017 (after removing the long-term linear trend and seasonal cycle). EOF2 accounts for 13.5% of the total variance. **b** Correlation map of the FMA SPQ index with concurrent SST anomalies. Positive (red) and negative (blue) values, with correlations significant at the 90% confidence level, are shaded. The FMA SPQ index is defined by the four green boxes [positive regression boxes: B (58°–36°S, 173°–145°W) and D (37°–17°S, 103°–76°W); negative regression boxes: A (47°–25°S, 142°E–179°W) and C (59°–40°S, 113°–81°W)]. **c** The normalized monthly VM indices (blue line) and SPQ indices (red line) as functions of time

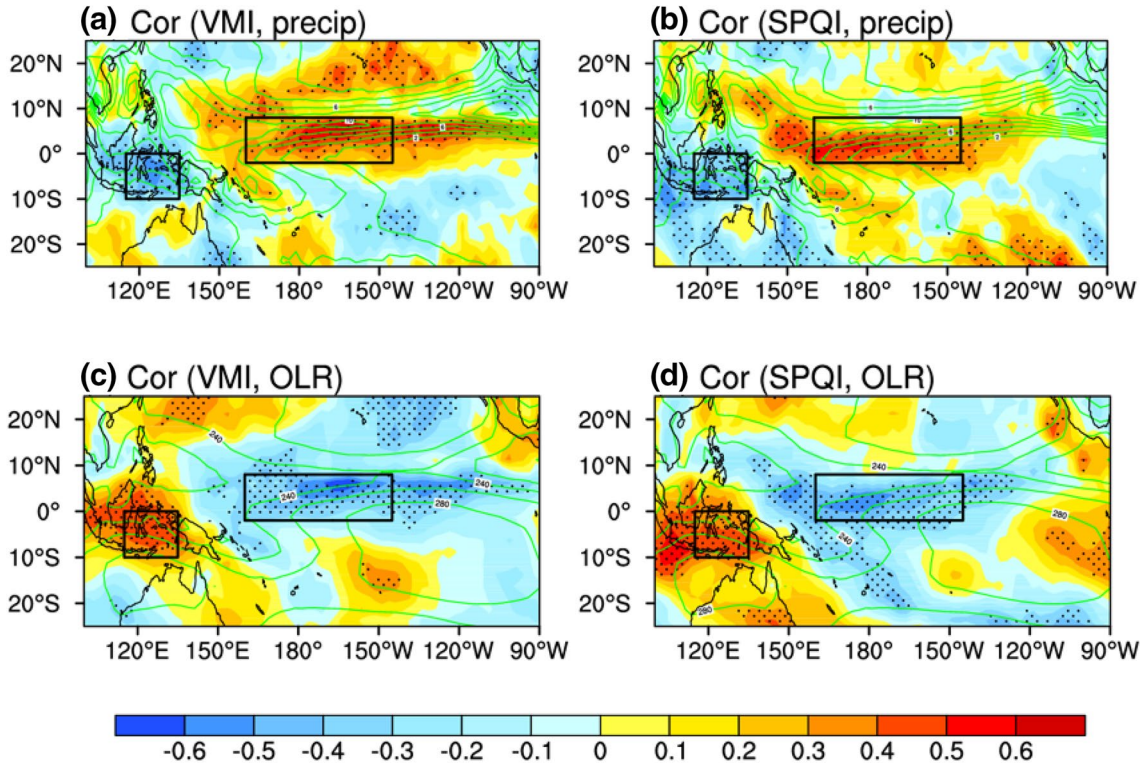

Fig. 2 **a** Correlation map of the FMA VMI with JJA precipitation anomalies based on the CMAP dataset. **b** As in **a** but for the correlations between the FMA SPQI and JJA precipitation anomalies. **c** Correlation map of the FMA VMI with JJA OLR anomalies. **d** As in **c** but for the correlations between the FMA SPQI and JJA OLR anomalies. In **a**–**d**, The climatological (1988–2017) boreal summer mean precipitation or OLR are indicated by contours. The two black boxes are the areas of positive correlations (2°N–8°N, 160°E–145°W) and negative correlations (10°S–0°, 115°E–135°E), which indicate the locations of the CP and WP regions, respectively. Correlations that exceed the 90% significance level are stippled

features can be obtained from the OLR field (Fig. 2c, d) and are consistent with the suppressed rainfall anomalies over the western Pacific and abundant central Pacific rainfall (Fig. 2a, b).

To test whether the VM and SPQ can interfere with each other, we analyze the joint relationship of the FAM VMI and SPQI on JJA Pacific ITCZ precipitation using scatterplots of the VMI and SPQI versus area-averaged precipitation anomalies over the western and central Pacific (WPI and CPI, respectively). The correlation coefficient between the FMA VMI and JJA western Pacific precipitation anomalies is higher when the VMI and SPQI have the same sign ($R = -0.68$; Fig. 3a) than when the VMI and SPQI have opposite signs ($R = -0.42$; Fig. 4a). Similarly, the correlation coefficient of the FMA SPQI with the JJA western Pacific precipitation anomalies also affected by the phase of VMI: it is -0.73 when the VMI and SPQI are in phase but only -0.11 when they are out of phase (Figs. 3b, 4b). In the central Pacific, we note that the correlation coefficient between the FMA VMI and JJA central Pacific precipitation anomalies is also high ($R = 0.65$; Fig. 3c) when the VMI and SPQI have the same sign, but the correlation coefficient is only 0.40 when they have opposite signs (Fig. 4c). In addition, the sign of the VMI can strongly affect the correlation coefficient between the FMA SPQI and JJA central Pacific precipitation anomalies, with correlations coefficient of 0.72 when the VMI and SPQI have the same sign and 0.18 when they have opposite signs (Figs. 3d, 4d). Compared with the correlation coefficient between the VMI and WPI or CPI, the correlation coefficient between the SPQI and WPI or CPI can vary to a greater extent with varying phase combinations of the VM and SPQ. The above correlation coefficients are also vividly displayed in Table 1 where it is easier to get the conclusion that the correlations between these two modes in northern and southern hemispheres and tropical precipitation are much stronger in VM/SPQ same-sign events than in opposite-sign events.

In addition, we measure the composite differences of 500-hPa JJA ω anomalies in same-sign and opposite-sign events over the two regions. In same-sign events, the composite differences are calculated by positive VM with positive SPQ events (VM+/SPQ+) minus negative VM with negative SPQ events (VM−/SPQ−). For opposite-sign events, we use positive VM with negative SPQ events (VM+/SPQ−)

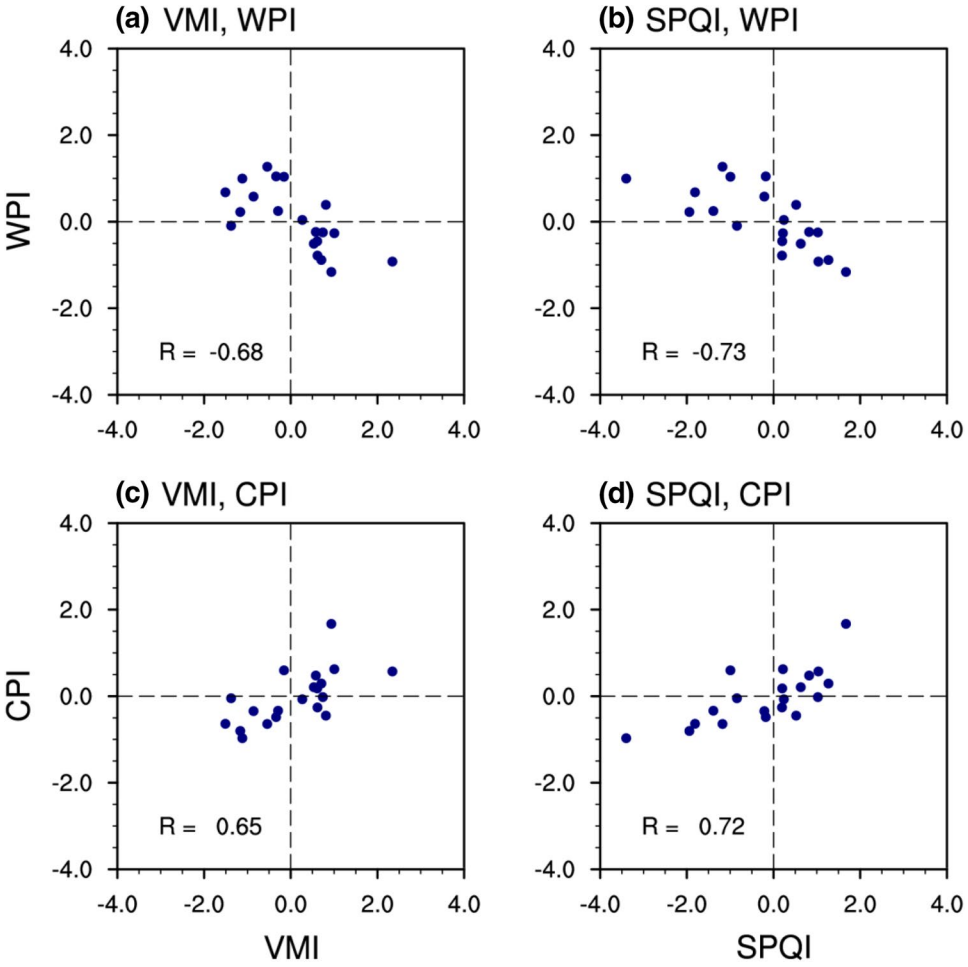

Fig. 3 Scatterplots of the **a** FMA VMI versus subsequent JJA WPI, **b** FMA SPQI versus subsequent JJA WPI, **c** FMA VMI versus subsequent JJA CPI, and **d** FMA VMI versus subsequent JJA CPI. Only years in which the VMI has the same sign as the SPQI are plotted. Correlation coefficients are included in each panel and all of them are significant at the 99% confidence level

minus negative VM with positive SPQ events (VM−/SPQ+) to calculate the composite differences. The strength of the ω, which can represent the convective activity, is significantly different between the two events, especially in the key study regions (Fig. 5a, b). In present study, the positive ω means downward motion and negative ω means upward motion. Over the western Pacific, negative anomalies are much stronger in same-sign events than in opposite-sign events. To quantitatively measure the strength of vertical velocity between the two events, we calculate the average value of ω in these two regions. For WP region, the mean value of vertical velocity in same-sign events is 1.68 10^{-2} Pa s^{-1}, compared with 0.25 10^{-2} Pa s^{-1} for opposite-sign events (Fig. 5e). Thus, there exists a significant sinking motion over the western tropical Pacific in same-sign events, whereas no such motion is evident in opposite-sign events. In the central Pacific (Fig. 5f), ascending motion is stronger in same-sign events (− 1.32 10^{-2} Pa s^{-1}) than in opposite-sign events (− 0.73 10^{-2} Pa s^{-1}). We perform the same analysis with OLR data to verify these results. The mean OLR values over the western tropical Pacific are 10.87 and 1.17 W m^{-2} for same-sign and opposite-sign events, respectively. The differences between the two events (− 9.34 and − 4.43 W m^{-2}, respectively) are also large over the central tropical Pacific. In conclusion, both ω and OLR have significant differences between same-sign and opposite-sign events over these two regions.

The above results suggest that the Pacific ITCZ summer precipitation anomalies are not only affected by the VM but also by the SPQ. When the VM and SPQ are in phase, their individual influence on Pacific ITCZ summer precipitation is enhanced. However, when the two modes are out of phase, they interfere with each other, causing a reduction in their influence on Pacific ITCZ summer precipitation.

4 Mechanism

In order to study the physical mechanism by which the FMA VM and SPQ jointly affect the subsequent summer tropical Pacific ITCZ precipitation anomalies, we show concurrent and lagged correlation maps of the FMA, AMJ, and JJA surface wind, SST, and precipitation anomalies with the FMA VMI for events in which the VMI and SPQI have the

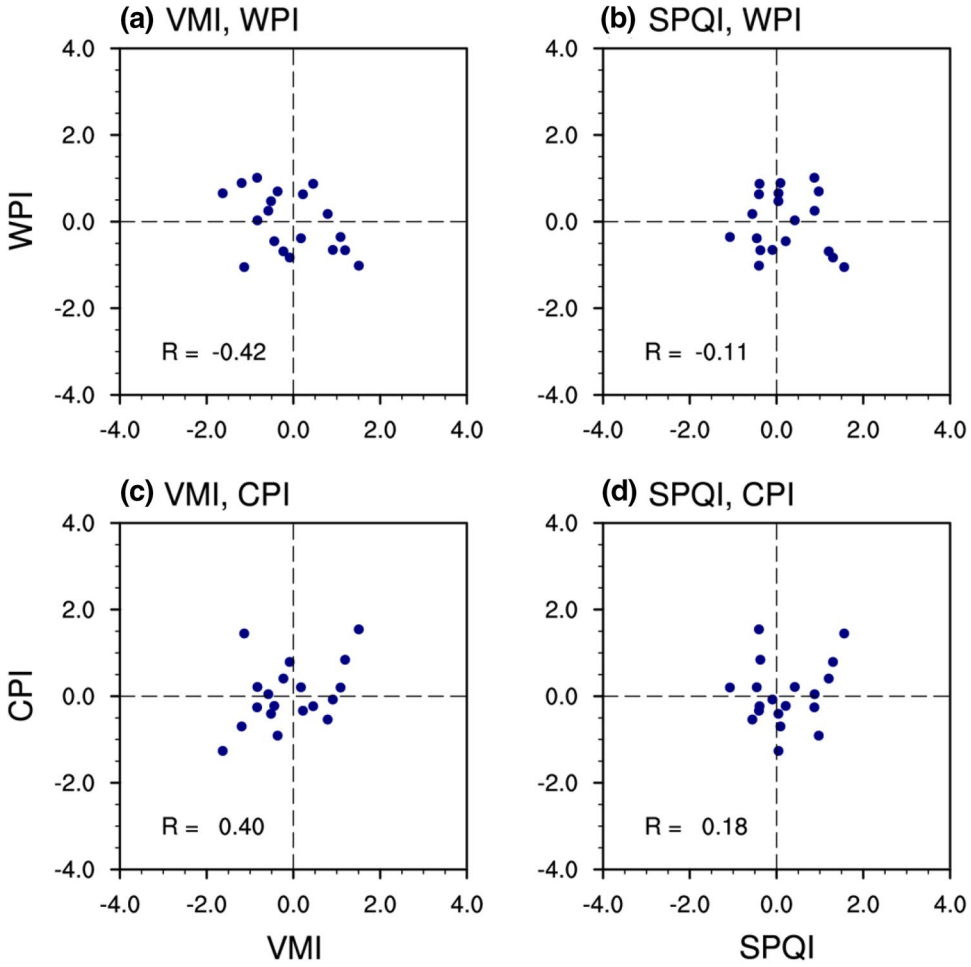

Fig. 4 As in Fig. 3, but for years in which the VMI has the opposite sign as the SPQI. And all of them are not significant at the 99% confidence level

Table 1 Correlation coefficients between VMI, SPQI and WPI, CPI

	WPI		CPI	
VMI	**– 0.68**	*– 0.42*	**0.65**	*0.40*
SPQI	**– 0.73**	*– 0.11*	**0.72**	*0.18*

The bold represents same sign VM/SPQ events, and the italics means opposite VM/SPQ events

same and opposite sign (Fig. 6). For same-sign VM/SPQ years, an anomalous circulation like the North Pacific Oscillation (Walker et al. 1932) during FMA generate a notable horseshoe-like SST pattern, with positive SST anomalies extending from the subtropical central–eastern North Pacific toward the equatorial central Pacific (Fig. 6a). Meanwhile, significant negative SST anomalies triggered by the PSA mode can be clearly captured around Australia in the southwestern Pacific. Thus, positive SST anomalies over the North western–central Pacific, combined with negative SST anomalies over the South western Pacific, produce a zonal SST gradient across the tropical western–central Pacific. The distinct SST gradient related to VM and SPQ results in westerly anomalies over the western–central tropical Pacific. As for central Pacific, the anomalous westerlies from the western–central tropical Pacific meet the anomalous easterlies from the eastern tropical Pacific, this low-level convergence then cause the convection motion and make the positive SST anomalies develop. Concurrently, anomalous westerlies to the east of the Maritime Continent cause divergence over the western Pacific and then strengthen negative SST anomalies in this region. As the season changes, the North Pacific horseshoe-like SST pattern persists (Fig. 6b), which subsequently leads the anomalous westerlies over the central Pacific develop and persist during JJA through WES mechanism (Fig. 6c). At this time, the significant negative SST anomalies in the southwestern Pacific also strengthen anomalous southwesterlies over the western tropical Pacific. Then, these westerly anomalies cause low-level divergence (convergence) over the western (central) Pacific, which promotes active downward (upward) motion in this region. This central-Pacific upward movement is collocated with the rising branch of local Hadley cells and enhances convection. The increase in convection and precipitation tend to make the release of condensed latent heat to the atmosphere

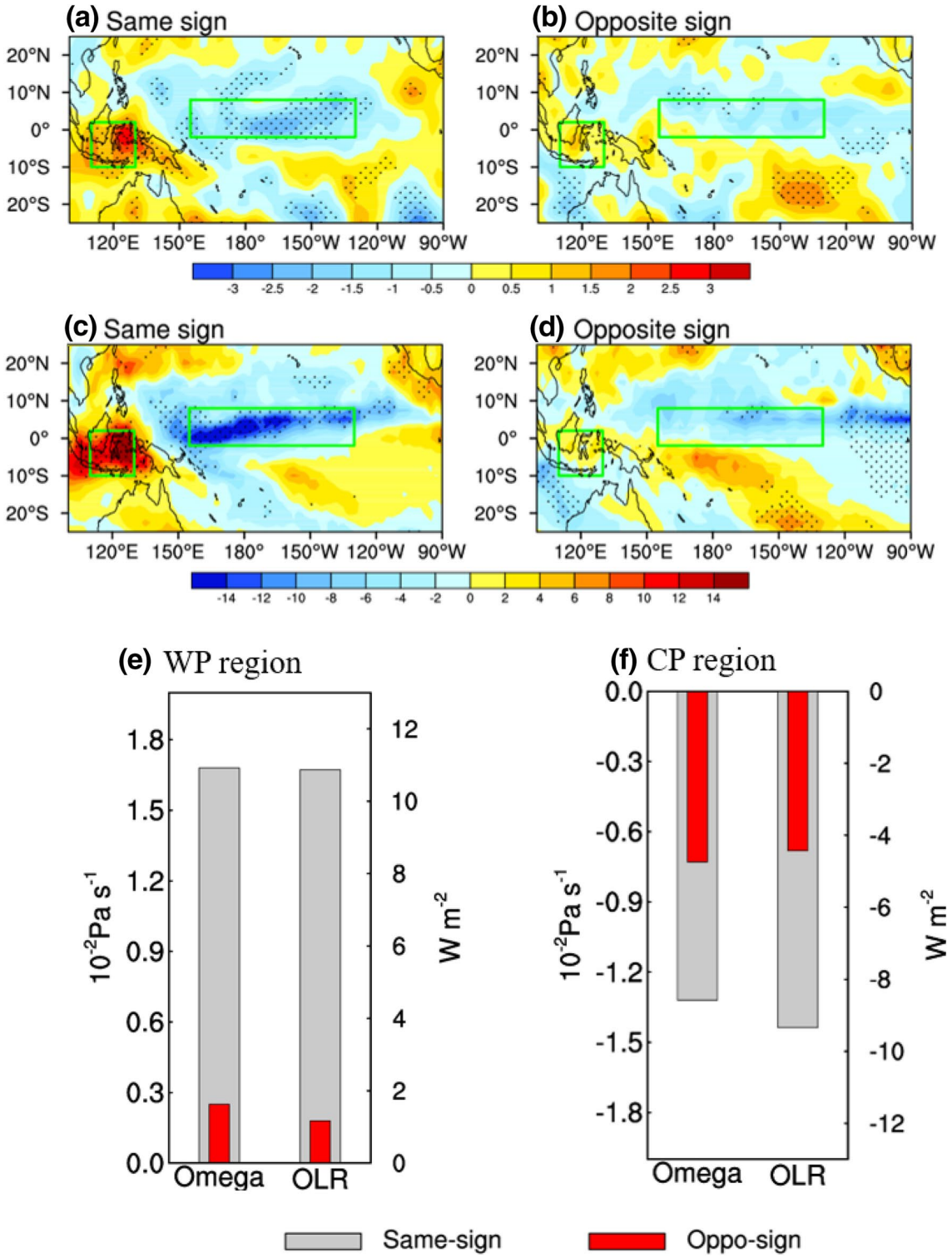

Fig. 5 **a** Composite differences in 500-hPa summer (JJA) vertical velocity (10^{-2}Pas^{-1}) anomalies between VM+/SPQ+ and VM−/SPQ− events. **b** Composite differences in 500-hPa summer (JJA) vertical velocity (10^{-2}Pas^{-1}) anomalies between VM+/SPQ− and VM−/SPQ+ events. **c**, **d** As in **a**, **b** but for composite differences in OLR (W m^{-2}) anomalies. Composite differences that exceed the 90% significance level are stippled. **e** Area-averaged strength of ω and OLR over the WP region. **f** As in **e** but for the CP region

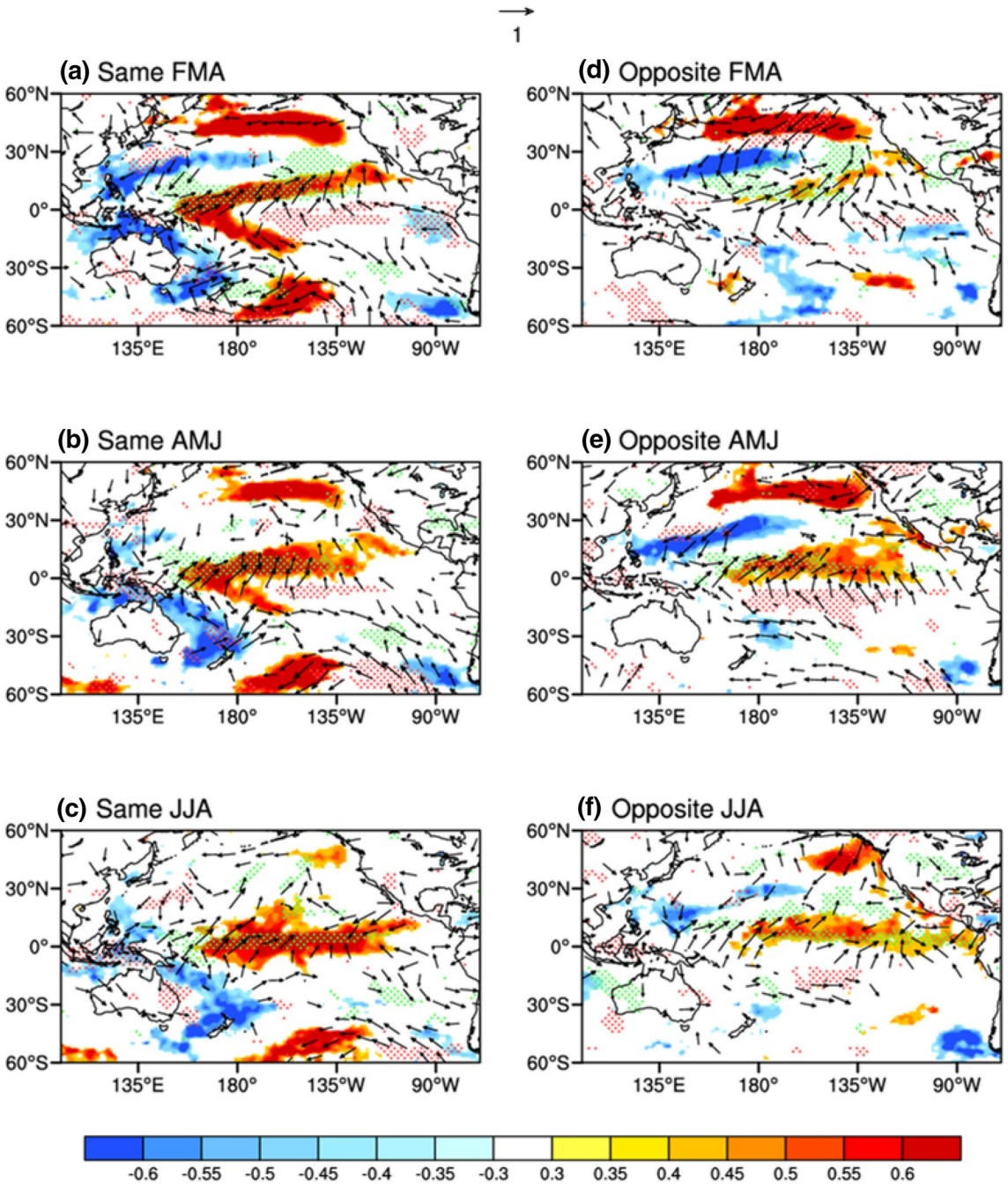

Fig. 6 Correlation maps of 3-month averaged SST (shading), surface wind (vectors) and precipitation (stippled) anomalies for FMA, AMJ, and JJA with the FMA VMI, calculated for years in which the VM and SPQ have the same (left panels) and opposite (right panels) signs. Positive (red) and negative (blue) SST anomalies with correlations significant at or above the 90% confidence level are shaded. Only surface wind vectors significant at the 90% confidence level are shown. Positive (green) and negative (red) precipitation anomalies with correlations significant at or above the 90% confidence level are stippled

increase, that then helps to enhance low-level convergence, upward movement, and convective precipitation. At the same time, abnormal high-level divergent winds move southwestward and converge over the western Pacific. This results in a downward movement that inhibits convection and reduces precipitation over the western Pacific.

For opposite-sign VM/SPQ events (Fig. 6d–f), the anomalous SST pattern related to the VM is weaker, and its subtropical positive SST anomalies does not extend far into the tropical region during FMA (Fig. 6d). The biggest difference in the South Pacific compared with same-sign events (Fig. 6a) is that positive SST anomalies (instead of

negative SST anomalies) appear around Australia because of the opposite SPQ phase (which are not significant above 90% confidence level). As a result, the tropical zonal SST gradient across the western–central Pacific weakens, which results in weaker abnormal westerly winds. Low-level convergence (divergence) over the central (western) Pacific becomes indistinct in opposite-sign events, thereby attenuating the development of anomalous precipitation in this region (Fig. 6f).

We also examine the correlations of the FMA, AMJ, and JJA surface wind, SST, and precipitation anomalies with late winter–early spring SPQ for years where the FMA VMI and SPQI have the same or opposite signs (Fig. 7). As found in the analysis described above, westerly anomalies over the western–central tropical Pacific are greatly enhanced in same-sign VM/SPQ events because the zonal SST gradient across the western–central tropical Pacific continues to exist (Fig. 7a). However, for opposite-sign VM/SPQ events, the

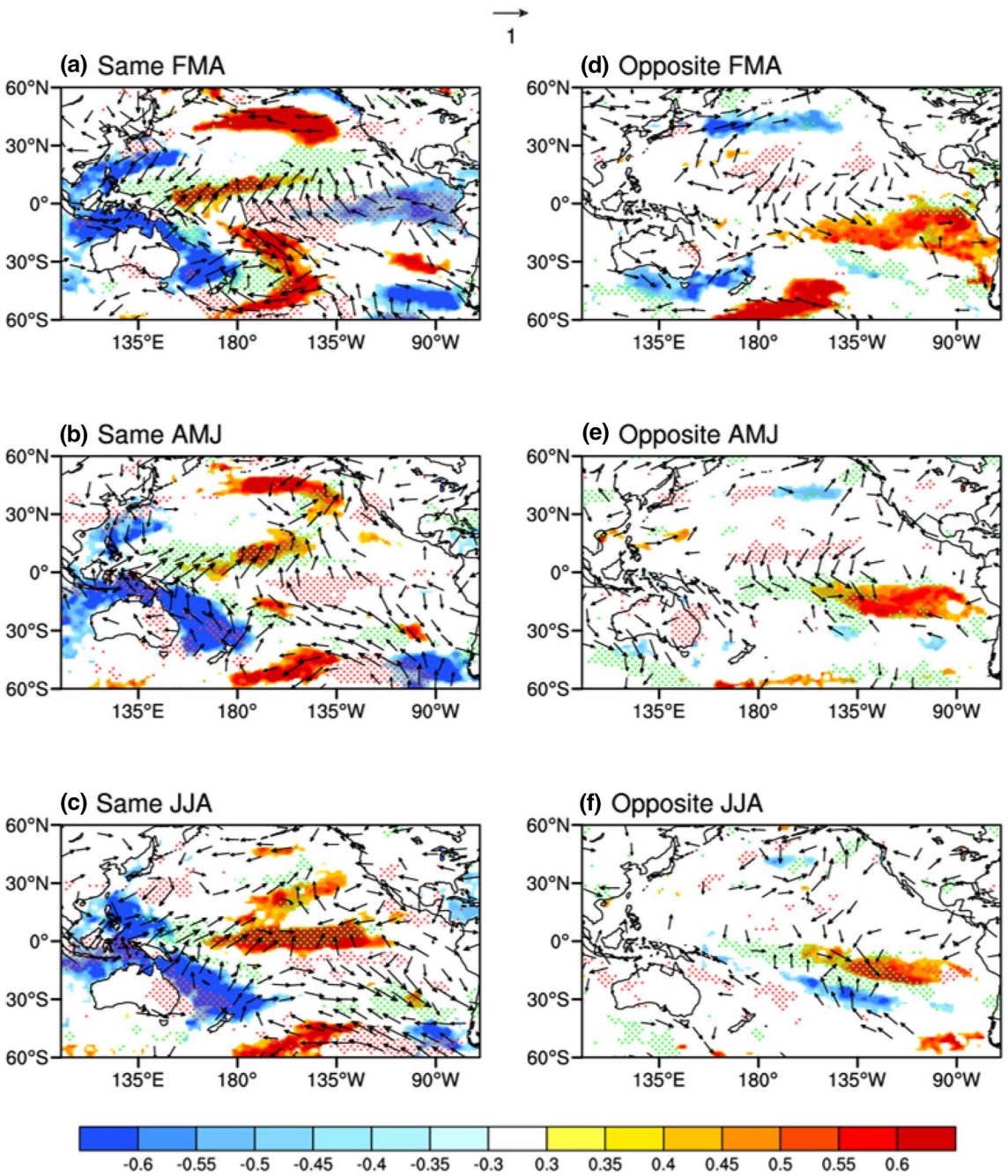

Fig. 7 As in Fig. 6, but for correlations with SPQI

central Pacific are covered by negative SST anomalies due to the negative VM, which do not exceed the 90% significance level (Fig. 7d). In South Pacific, negative SST anomalies still exist (but weaker) around Australia. Hence, the tropical zonal SST gradient across the western–central Pacific is reduced because of the positive-to-negative change in central Pacific SST anomalies which related to the VM. The anomalous westerlies are also reduced as a result of the weakened zonal SST gradient, which is not favorable for low-level convergence (divergence) over the eastern–central (western) Pacific and associated anomalous precipitation (Fig. 7f).

5 Model simulations

To further confirm that different phase combinations of VM and SPQ can have different influences on precipitation over the western and central Pacific, we analyze the output of 25 individual models from CMIP5 (Table 2). Basic works have confirmed that these 25 CMIP5 models can simulate the VM and SPQ well which are not shown here.

Figure 8a shows the correlation coefficients between the FMA VMI and the JJA WPI. Most models capture the higher correlation coefficients in same-sign events and the lower correlation coefficients in opposite-sign events. The multimodel ensemble mean (MME) is consistent with the individual model results. Figure 8b displays the correlation coefficients between the FMA SPQI and the JJA WPI for 25 models and the MME. These individual models and MME results have correlation coefficients for same-sign events that are much higher than those of opposite-sign events. Figure 8c, d is similar to Fig. 8a, b, but show correlation coefficients with CPI. The higher correlation coefficients for same-sign events and lower correlation coefficients for opposite-sign events support the finding that the competing impacts of the VM and SPQ on Pacific ITCZ summer precipitation can lead to a reduced net influence. In summary, most CMIP5 model simulations capture the patterns found in observations and support the conclusions drawn here.

Figure 8e presents the composite differences of JJA WPI between VM+/SPQ+ and VM−/SPQ− events and the composite differences of JJA WPI between VM+/SPQ− and VM−/SPQ+ events. For most models (21 out of

Table 2 List of the CMIP5 models used in this study

Number	Model name	Model center	Atmosphere (ocean) variable resolution (lon × lat)
1	ACCESS1-0	CSIRO-BOM/Australia	192 × 145 (360 × 300)
2	bcc-csm1-1-m	BCC/China	320 × 160 (360 × 232)
3	CanESM2	CCCma/Canada	128 × 64 (256 × 192)
4	CCSM4	NCAR/United States	288 × 192 (320 × 384)
5	CESM1-BGC	NCAR/United States	288 × 192 (320 × 384)
6	CESM1-FASTCHEM	NCAR/United States	288 × 192 (320 × 384)
7	CESM1-WACCM	NCAR/United States	144 × 96 (320 × 384)
8	CMCC-CM	CMCC/Italy	480 × 240 (182 × 149)
9	CMCC-CMS	CMCC/Italy	192 × 96 (182 × 149)
10	CNRM-CM5	CNRM-CERFACS/France	256 × 128 (362 × 292)
11	EC-EARTH	ICHEC/Ireland	320 × 160(362 × 292)
12	FGOALS-g2	LASG-IAP/China	128 × 60 (360 × 196)
13	FIO-ESM	FIO/China	128 × 64 (320 × 384)
14	GFDL-CM3	NOAA GFDL/United States	144 × 90 (360 × 200)
15	GFDL-ESM2G	NOAA GFDL/United States	144 × 90 (360 × 210)
16	GISS-E2-R-CC	NASA GISS/United States	144 × 90 (144 × 90)
17	HadGEM2-CC	MOHC/UK	144 × 192 (360 × 216)
18	HadGEM2-ES	MOHC/UK	144 × 192 (360 × 216)
19	inmcm4	INM/Russia	180 × 120 (360 × 340)
20	IPSL-CM5A-LR	IPSL/France	96 × 96 (182 × 149)
21	IPSL-CM5A-MR	IPSL/France	144 × 143 (182 × 149)
22	IPSL-CM5B-LR	IPSL/France	96 × 96 (182 × 149)
23	MIROC-ESM	MIROC/Japan	256 × 128 (256 × 192)
24	NorESM1-M	NCC/Norway	144 × 96 (320 × 384)
25	NorESM1-ME	NCC/Norway	144 × 96 (320 × 384)

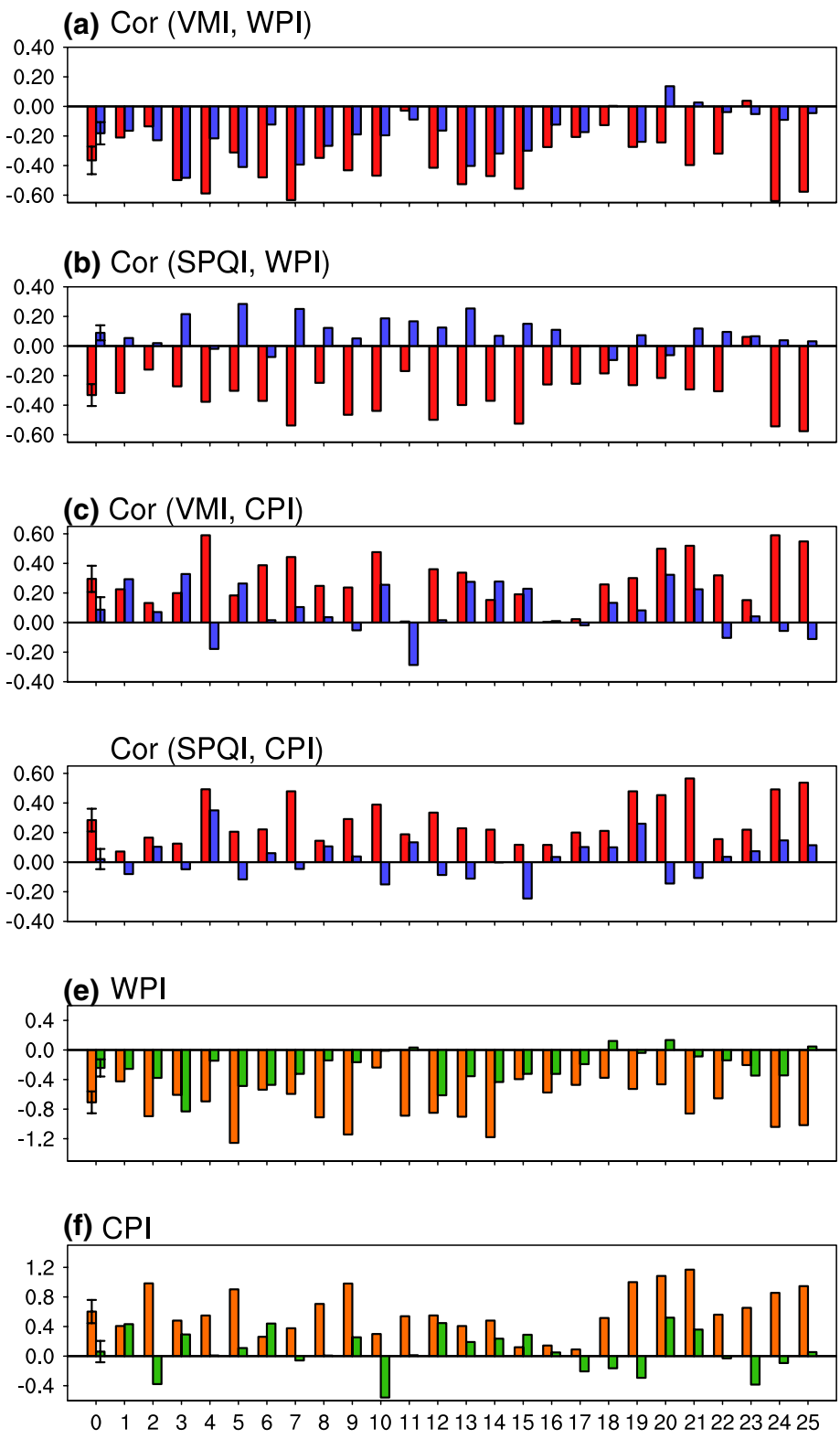

Fig. 8 Correlation coefficients of the **a**, **c** FMA VMI and **b**, **d** FMA SPQI with subsequent **a**, **b** WPI and **c**, **d** CPI in 25 CMIP5 models and the multimodel ensemble mean (MME) of 25 CMIP5 models. Red (blue) bars indicate years in which the VM has the same (opposite) sign as the SPQ. **e** Composite differences of WPI between VM+/SPQ+ events and VM−/SPQ− events (orange bars) and between VM+/SPQ− events and VM−/SPQ+ events (green bars) for 25 individual models and MME. **f** As in **e** but for composite differences of CPI. Vertical error bars indicate 0.5 standard deviation of inter-model variability. Number 0 represent MME and numbers 1–25 represent the 25 CMIP5 models listed in Table 2

25), WPI strength in same-sign events is much stronger than in opposite-sign events. WPI values are negative in same-sign events, which indicates that the individual influences of VM and SPQ are strengthened. In opposite-sign events, WPI values become positive in four models, which indicates that the influences of VM and SPQ compete and lead to indistinct precipitation anomalies over the western Pacific. We also calculate the MME of the 25 models and find that

the mean strength in same-sign events is significantly greater than in opposite-sign events. Figure 8f displays the composite differences of JJA CPI between VM+/SPQ+ and VM−/SPQ− events and the composite differences of JJA WPI between positive VM+/SPQ− and VM−/SPQ+ events. There are 20 models that perform well in simulating the differences between same-sign and opposite-sign events. In these 20 models, the CPI strength in same-sign events is much greater than in opposite-sign events. The weaker CPI and changes of CPI sign (positive-to-negative) during VM+/SPQ− and VM−/SPQ+ events further confirm the opposing effects of VM and SPQ on Pacific ITCZ summer precipitation.

The results presented above indicate that the CMIP5 model captures well the interdependence of the late winter–early spring VM and the SPQ in affecting following summer Pacific ITCZ precipitation. Next, we use the MME of these models to analyze the evolution of FMA, AMJ, JJA surface wind, SST, and rainfall anomalies for events with four distinct combinations of VM and SPQ. In the VM+/SPQ+ events (Fig. 9a–c), there are positive SST anomalies in the central Pacific, and ocean regions to the north and east of Australia are covered by cold SST anomalies. These conditions are both favorable for zonal SST gradients and anomalous westerlies across the western–central Pacific. This leads to significant positive precipitation anomalies in the central Pacific while marked negative precipitation anomalies occur in the western Pacific. The 3-month evolution of the VM−/SPQ− events (Fig. 9d–f) is almost opposite that of the VM+/SPQ+ events. As shown in Fig. 9g, there

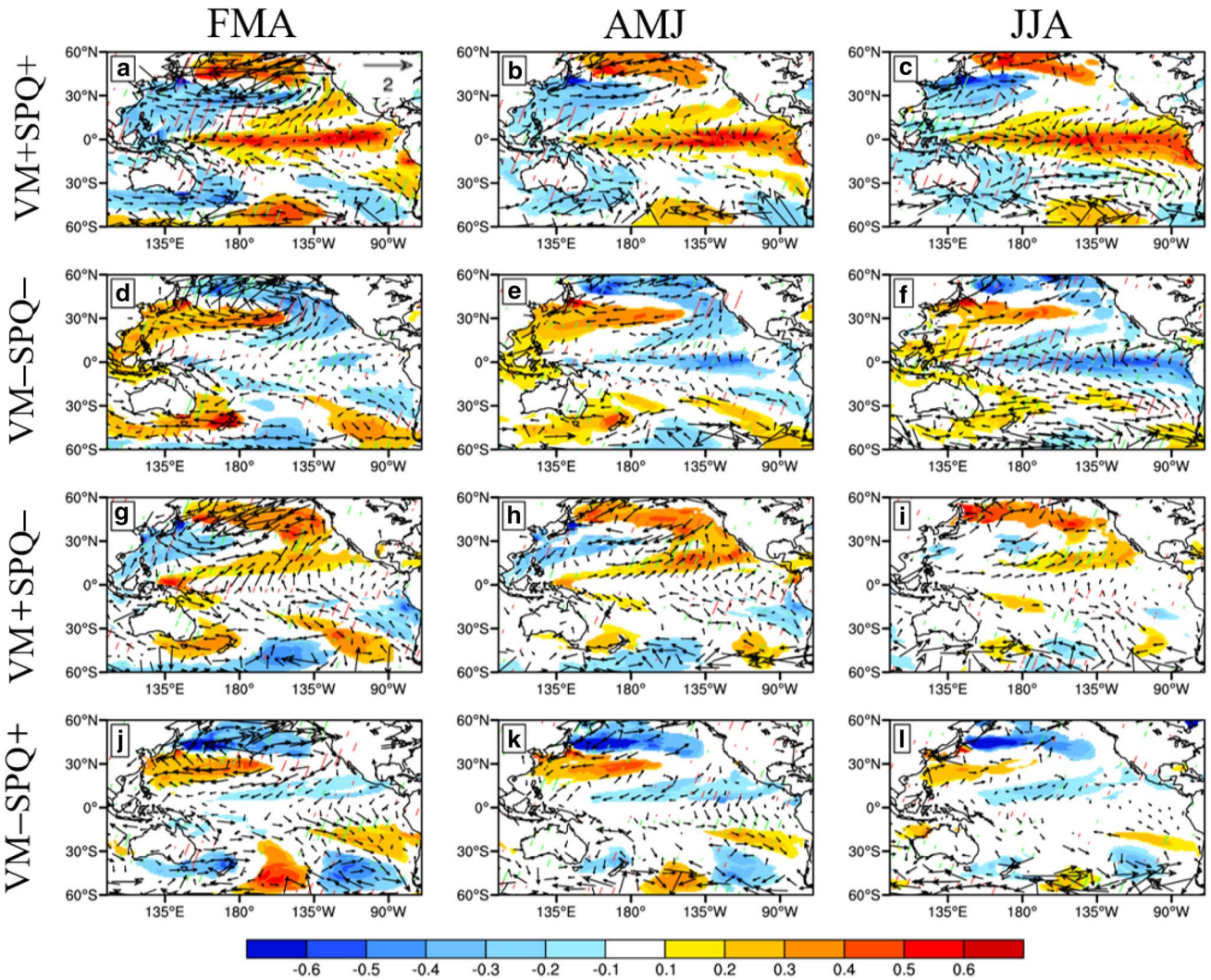

Fig. 9 Composite of the MME 3-month averaged SST (°C; shading), surface wind (m/s; vectors) and precipitation (mm day^{-1}; hatching) anomalies in four different VM and SPQ phase combinations (top to bottom) for 25 CMIP5 models for FMA, AMJ and JJA (left to right). For precipitation, green indicates positive anomalies and red indicates negative anomalies. Only SST, surface wind and precipitation anomalies significant at the 90% confidence level are shown

are also positive SST anomalies in the North Pacific, but the anomalous SST in the South Pacific are completely different, and warm SST anomalies around Australia do not produce a zonal SST gradient. The influences of the North and South Pacific compete with each other, and thus there are no significant SST anomalies a season later, and undoubtedly no significant precipitation anomalies. Figure 9j–l shows the evolution in the VM−/SPQ+ events, revealing that SST anomalies related to the VM suppress the formation of westerly anomalies and that there is no significant ITCZ precipitation during JJA.

These results from most CMIP5 models indicate that the physical processes underlying the VM and SPQ involvement in ITCZ summer anomalous precipitation for same-sign and opposite-sign VM/SPQ years are significantly different, and are generally similar to the processes indicated by observations.

6 Prediction model

The results shown above reveal that the capability of the VM or the SPQ to influence following Pacific ITCZ precipitation depends on the phase of the other. In addition, the correlation coefficient between the FMA VMI and SPQI is relatively weak, which suggests that the VM and the SPQ are relatively independent of each other. Considering their tight relationship in predicting precipitation over the two regions, two empirical models are established to predict the boreal summer WPI and CPI (referred to as WPI_{JJA} and CPI_{JJA}, respectively) based on both the FMA VMI and FMA SPQI (referred to as VMI_{FMA} and $SPQI_{FMA}$, respectively):

$$WPI_{JJA} = a_1 \times VMI_{FMA} + b_1 \times SPQI_{FMA} \text{ and} \quad (1)$$

$$CPI_{JJA} = a_2 \times VMI_{FMA} + b_2 \times SPQI_{FMA}. \quad (2)$$

The parameters $a_1 = -0.45$ and $b_1 = -0.36$, and $a_2 = 0.46$ and $b_2 = 0.34$ are calculated by a least-squares fit to the VMI_{FMA} and $SPQI_{FMA}$, respectively. To assess the prediction skills of these two models, we compare the predicted JJA WPI and JJA CPI with observations. There is a high correlation coefficient (R = 0.66) between the observed JJA WPI and those predicted by model (1), which is higher than for the single VMI model (R = 0.56) and single SPQI model (R = 0.50; Fig. 10a). The root-mean-squared error (RMSE) between the observed JJA WPI and that predicted by model (1) is 0.55, which is smaller than that for the single VMI model (0.59) and single SPQI model (0.62; Fig. 10a). For central Pacific (Fig. 10b), the correlation coefficient between the observed JJA CPI and that predicted by model (2) is 0.61, which is higher than that of the single-factor VMI (0.51) and the single-factor SPQI (0.60). The RMSE calculated from model (2) is also smaller (0.55) than those from the single VMI model (0.59) and the single SPQI model (0.60). These results indicate that the combination of both the VM and SPQ has better prediction skills for JJA WPI and CPI than do the single-factor models.

Although models (1) and (2) have relatively high prediction skill, we cannot ignore the influence of ENSO, which is the most important interannual signal around the world. As the Niño3.4 index reaches its peak during boreal winter, calculated as the area-averaged SST over the Niño3.4 region (5°S–5°N, 170°–120°W), we use the previous-winter Niño3.4 index (December–February) (Trenberth and Stepaniak 2000) to build an empirical prediction model for JJA ITCZ precipitation. The prediction skills of the single Niño3.4 index are shown in Fig. 10a, b. The correlation coefficients for both the western and central Pacific regions are very small (0.02 and 0.07, respectively), which means that the single preceding Niño3.4 index is not useful for predictions of JJA ITCZ precipitation.

We also add the Niño3.4 index into models (1) and (2) to establish new models (3) and (4):

$$WPI_{JJA} = a_3 \times VMI_{FMA} + b_3 \times SPQI_{FMA} + c_3 \times NINO3.4_{DJF} \text{ and} \quad (3)$$

$$CPI_{JJA} = a_4 \times VMI_{FMA} + b_4 \times SPQI_{FMA} + c_4 \times NINO3.4_{DJF}. \quad (4)$$

The correlation coefficients and RMSE of models (3) and (4) are almost the same as those of models (1) and (2), as shown in Fig. 10a, b. This means that the addition of the Niño3.4 index does not improve predictions of summer precipitation over these two areas. Therefore, the optimal choice for predictions of Pacific ITCZ summer precipitation is the use of a combination of the FMA VMI and SPQI, as used in models (1) and (2).

To further evaluate the prediction skills of models using both the VMI and SPQI, we perform several hindcast experiments. First, we use a leave-one-out method, which is to repeatedly delete 1 year during 1979–2017, and then establish a linear regression model with the FMA VMI and SPQI based on the remaining data, and finally hindcast the missing year. As shown in Fig. 11b, the correlations between the observed values and cross-validated hindcasts are somewhat lower than those shown in Fig. 11a, but are still statistically significant in the key regions we focus on (including the WP and CP regions).

A holdout method is also applied to a set of hindcast experiments in which the whole time series is divided into two parts: a training period and a hindcasting period. We establish the model based on historical data from 1979 to 2000, and predict the JJA WPI and CPI from 2001 to 2017. High correlation coefficients and relatively small RMSE between the hindcast and observed WPI and CPI are obtained for these hindcast

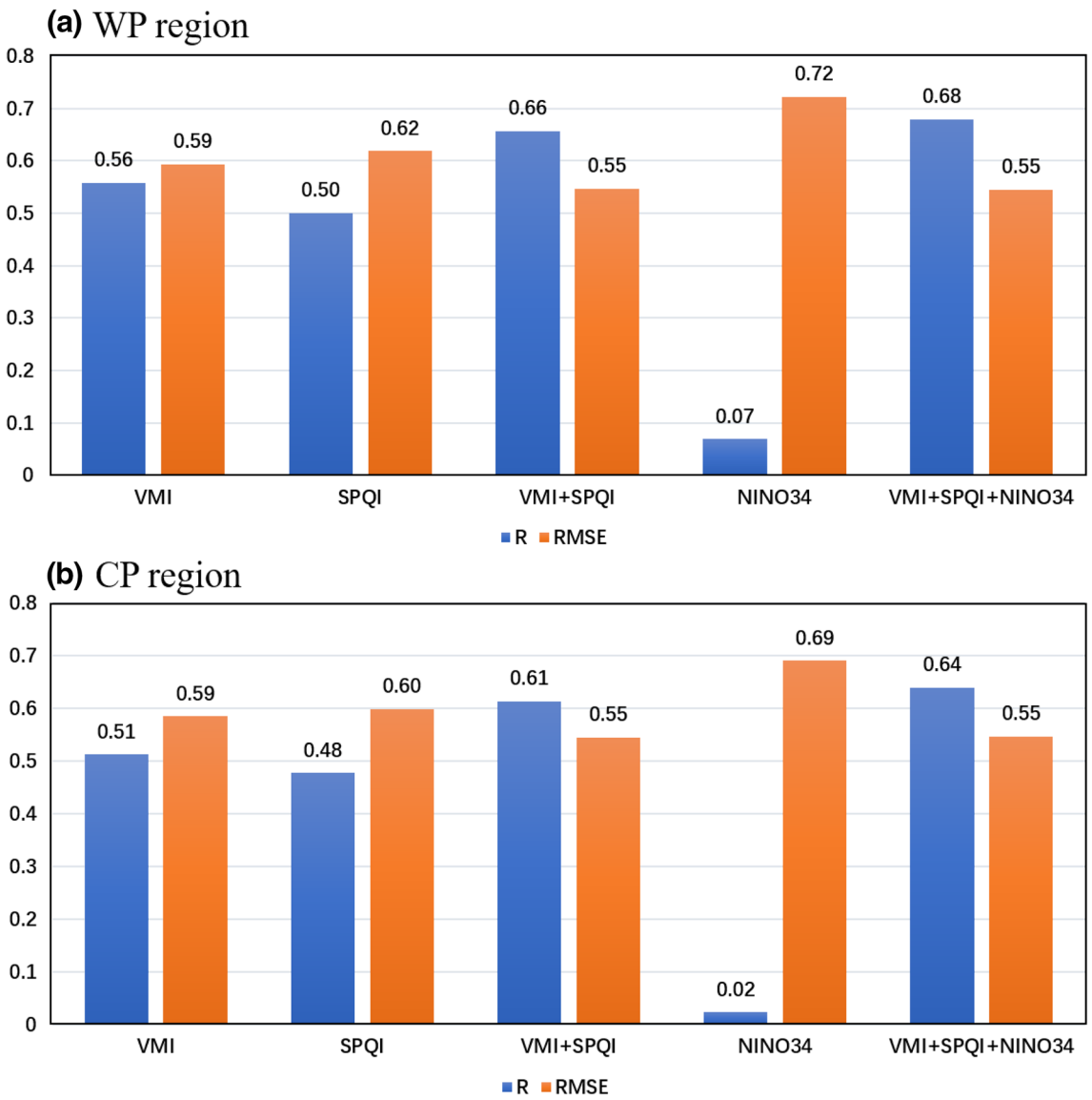

Fig. 10 Prediction skills of 5 empirical models for Pacific ITCZ summer precipitation for the period 1979–2017. **a** Correlation coefficients (blue bars) and root-mean-squared errors (RMSE; orange bars) between observed and predicted JJA WPI for different empirical models (VMI, SPQI, VMI + SPQI, NINO34, and VMI + SPQI + NINO34). **b** As in **a** but for predictions of the JJA CPI

experiments (Fig. 11c, d). Therefore, this model can be used to accurately simulate ITCZ summer precipitation.

These hindcast experiments to the models prove that the VM and SPQ are essential precursors of summer precipitation over the western and central tropical Pacific. Their joint use improves prediction skills more than does their individual use.

7 Summary and discussion

Our research examines the joint relationship of the VM and SPQ with Pacific ITCZ summer precipitation. We find that the relationship of VM with subsequent Pacific ITCZ summer precipitation intensity may strongly depend on the state of concurrent SPQ, and vice versa. When boreal late winter–early spring VM and SPQ have opposite signs, their individual correlations with subsequent Pacific ITCZ summer precipitation anomalies become much smaller, and the precipitation, OLR, and vertical motion also tend to be weaker. However, these correlations become significantly stronger when the two sets of anomalies have the same sign. The strength of the precipitation, OLR, and vertical motion also tend to be stronger under these conditions.

The possible reason for this relationship is that due to the competing SST anomalies resulting from the VM and the SPQ, the anomalous westerly in the western–central

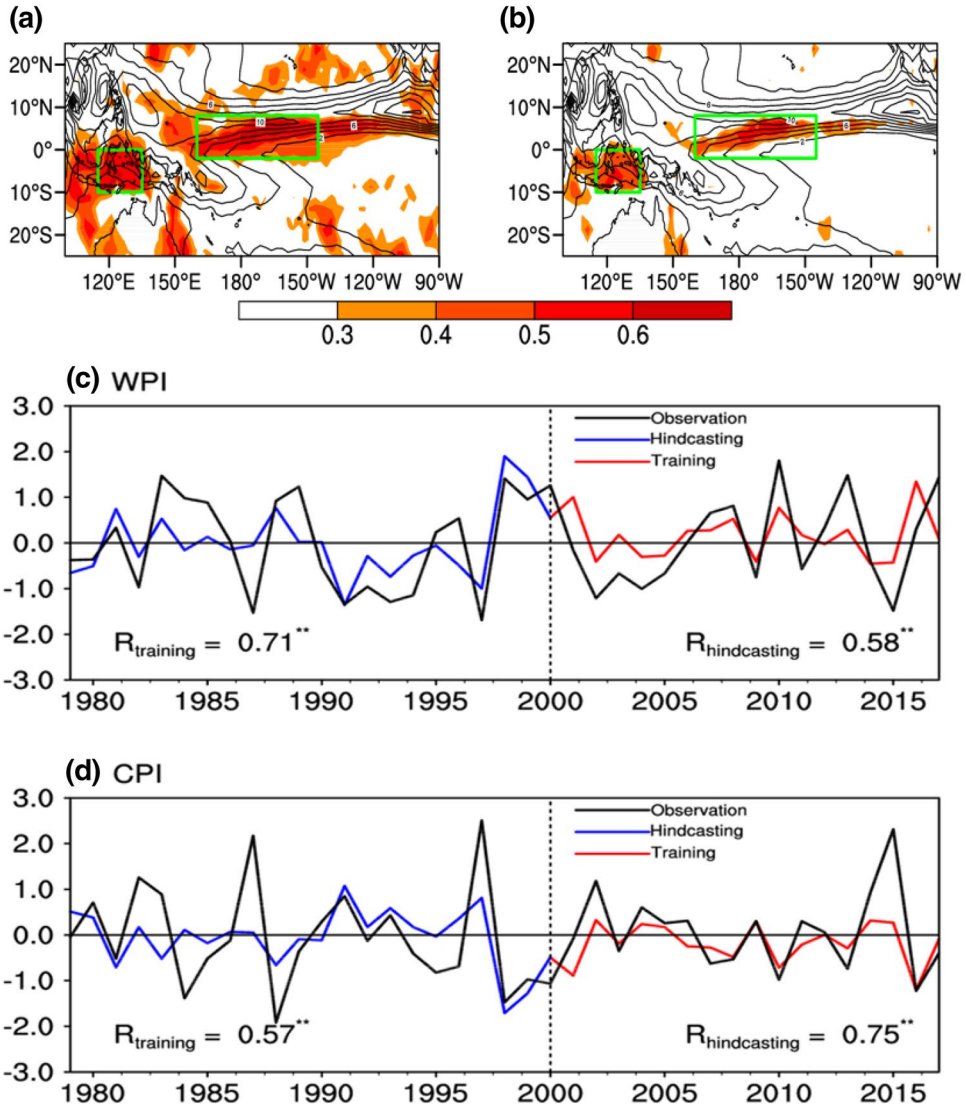

Fig. 11 **a** Correlation between observed and hindcasted summer (JJA) precipitation anomalies obtained from the empirical prediction model with VMI and SPQI. **b** Correlations between observations and cross-validated hindcasts of JJA precipitation anomalies. Only areas with correlations significant at the 90% level are shown. The climatological (1981–2010) summer mean precipitation (mm day^{-1}) is shown as contours. **c** JJA WPI from observations (black line; 1979–2017), the training period (blue line; 1979–2000) and the hindcasting period (red line; 2001–2017). **d** As in **c** but for JJA CPI. **99% confidence level

tropical are strengthened/weakened during the same-sign and opposite-sign events, which is favoring/suppressing the development of Pacific ITCZ summer precipitation. Figure 12 presents a schematic diagram of the various processes that result in different ITCZ summer precipitation anomalies for same-sign and opposite-sign events. When the VM and SPQ both have positive signs, the SST pattern associated with VM+ events result in an eastward zonal SST gradient and anomalous westerlies, the SST pattern associated with SPQ+ events also generate an eastward zonal SST gradient and anomalous westerlies. Anomalous westerlies over the tropical western–central Pacific are thus strengthened. These strengthened westerlies cause convergence over the central Pacific and naturally bring about divergence over the western Pacific. Low-level convergence may further cause deep convection and enhanced precipitation, whereas low-level divergence may lead to suppressed convection and reduced precipitation. In opposite-sign events, the SST pattern associated with VM+ events generate an eastward zonal SST gradient and anomalous westerlies, but the SST pattern associated with SPQ− events generates a westward zonal SST gradient and anomalous easterlies. Therefore, opposing westerly anomalies in the North Pacific and easterly anomalies in the South Pacific weaken the anomalous westerlies over the tropical western–central Pacific. These weakened westerly anomalies lead to a decrease in convection and precipitation over both the western and central Pacific.

A set of CMIP5 model simulations confirm that the influence of the VM on Pacific ITCZ summer precipitation either constructively or destructively interferes with the corresponding influence of the SPQ. Most models show a higher correlation between the two precursors and Pacific ITCZ summer precipitation when the VM and SPQ have the same sign than when they have opposite signs. An analysis of the evolution of SST, wind, and precipitation using CMIP5 model data also indicates that our results

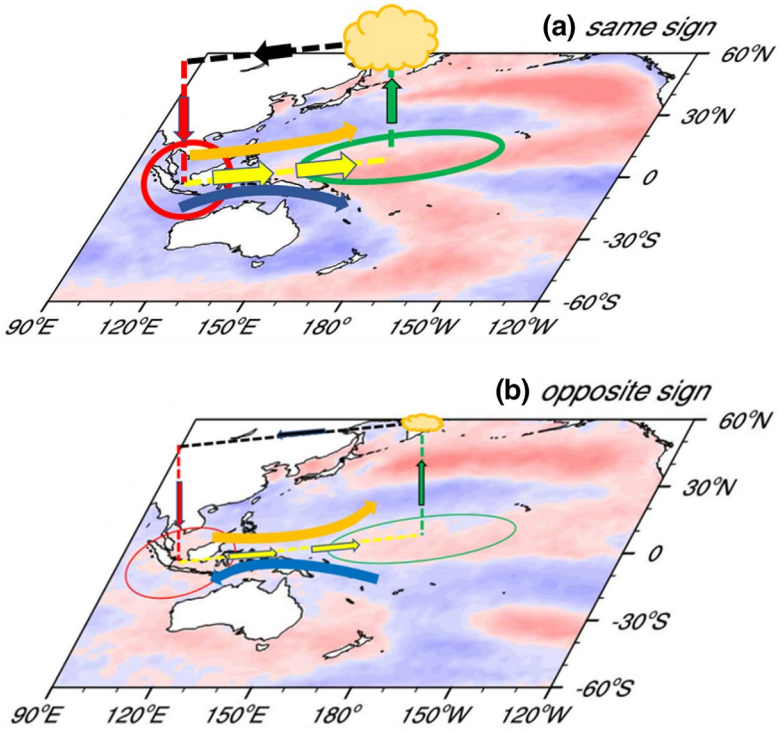

Fig. 12 Schematic representation of the thermodynamic ocean–atmosphere coupling between the ITCZ and SST anomalies associated with two different combinations of VM and SPQ. **a** Same sign events. The orange (blue) arrow represents zonal SST gradients generated by VM (SPQ). Thick yellow vectors denote strong anomalous westerlies affected by North and South Pacific zonal SST gradients. The green (red) line with thick green (red) vectors indicates strong upward (downward) motion. The thick green (red) ellipse represents the low-level convergence (divergence) region. The cloud indicates positive precipitation anomalies over the tropical central Pacific, and the black line with a thick black vector indicates anomalous upper circulation. **b** Opposite sign events. The blue arrow represents zonal SST gradients generated by SPQ, which are in the opposite direction as that in **a**. All thin vectors and lines are as in **a** but of weaker strength

derived from observations are robust. Note that the conclusions drawn here should be further verified using numerical simulations, such as the Community Earth System Model (CESM).

We have demonstrated that the VM and SPQ are important precursors to subsequent ITCZ summer precipitation, and we have built two empirical models to predict precipitation anomalies over the central and western Pacific. Applying a leave-one-out hindcast and a holdout hindcast, we demonstrate the high prediction skills of these models. Thus, the FMA VMI and SPQI are useful in predictions of ITCZ summer precipitation 4 months later.

Apart from the SST signal from the extratropical North and South Pacific, signals from other oceans should also be investigated for their ability to improve prediction skills for ITCZ summer precipitation. For example, the Indian Ocean dipole (Saji et al. 1999) and North American dipole (Ding et al. 2016) also have significant influences on the tropical Pacific (Ding et al. 2016, 2019; Stuecker et al. 2017; Zhou et al. 2019), and their roles in Pacific ITCZ summer precipitation should be further analyzed.

Acknowledgements This work was jointly supported by the National Natural Science Foundation of China (Grant No. 41790474) and the 973 project of China (2016YFA0601801).

References

Adam O, Bischoff T, Schneider T (2016) Seasonal and interannual variations of the energy flux equator and ITCZ. Part II: zonally varying shifts of the ITCZ. J Clim 29:7281–7293

Adler RF et al (2003) The version-2 global precipitation climatology project (GPCP) monthly precipitation analysis (1979–present). J Hydrometeorol 4:1147–1167

Bain CL, De Paz J, Kramer J, Magnusdottir G, Smyth P, Stern H, Wang C-C (2011) Detecting the ITCZ in instantaneous satellite data using spatiotemporal statistical modeling: ITCZ climatology in the East Pacific. J Clim 24:216–230

Bjerknes J (1969) Atmospheric teleconnections from the equatorial Pacific. Mon Weather Rev 97:163–172

Bond N, Overland J, Spillane M, Stabeno P (2003) Recent shifts in the state of the North Pacific. Geophys Res Lett 30:2183. https://doi.org/10.1029/2003GL018597

Broccoli AJ, Dahl KA, Stouffer RJ (2006) Response of the ITCZ to Northern Hemisphere cooling. Geophys Res Lett. https://doi.org/10.1029/2005GL024546

Castelli E, Papandrea E, Valeri M, Greco FP, Ventrucci M, Casadio S, Dinelli BM (2018) ITCZ trend analysis via Geodesic P-spline smoothing of the AIRWAVE TCWV and cloud frequency datasets. Atmos Res 214:228–238. https://doi.org/10.1016/j.atmosres.2018.07.019

Cheng H, Sinha A, Wang X, Cruz FW, Edwards RL (2012) The Global Paleomonsoon as seen through speleothem records from Asia and the Americas. Clim Dyn 39:1045–1062

Chiang JCH (2002) Deconstructing Atlantic Intertropical Convergence Zone variability: influence of the local cross-equatorial sea surface temperature gradient and remote forcing from the eastern equatorial Pacific. J Geophys Res. https://doi.org/10.1029/2000JD000307

Chiang JCH, Bitz CM (2005) Influence of high latitude ice cover on the marine Intertropical Convergence Zone. Clim Dyn 25:477–496. https://doi.org/10.1007/s00382-005-0040-5

Chiang JCH, Biasutti M, Battisti DS (2003) Sensitivity of the Atlantic Intertropical Convergence Zone to Last Glacial Maximum boundary conditions. Paleoceanography. https://doi.org/10.1029/2003PA000916

Chou C, Lo M-H (2007) Asymmetric responses of tropical precipitation during ENSO. J Clim 20:3411–3433. https://doi.org/10.1175/JCLI4197.1

Clement AC, Hall A, Broccoli A (2004) The importance of precessional signals in the tropical climate. Clim Dyn 22:327–341

Dai A, Wigley TML (2000) Global patterns of ENSO-induced precipitation. Geophys Res Lett 27:1283–1286. https://doi.org/10.1029/1999GL011140

Ding R, Li J, Tseng Y-h (2014) The impact of South Pacific extratropical forcing on ENSO and comparisons with the North Pacific. Clim Dyn 44:2017–2034. https://doi.org/10.1007/s00382-014-2303-5

Ding R, Li J, Tseng Y-h, Ruan C (2015a) Influence of the North Pacific Victoria mode on the Pacific ITCZ summer precipitation. J Geophys Res 120:964–979. https://doi.org/10.1002/2014JD022364

Ding R, Li J, Tseng Y-h, Sun C, Guo Y (2015b) The Victoria mode in the North Pacific linking extratropical sea level pressure variations to ENSO. J Geophys Res 120:27–45. https://doi.org/10.1002/2014JD022221

Ding R, Li J, Tseng Y-h, Sun C, Zheng F (2016) Linking a sea level pressure anomaly dipole over North America to the central Pacific El Niño. Clim Dyn 49:1321–1339. https://doi.org/10.1007/s00382-016-3389-8

Ding R, Li J, Tseng Yh, Sun C, Li Y, Xing N, Li X (2019) Linking the North American Dipole to the Pacific Meridional mode. J Geophys Res 124:3020–3034. https://doi.org/10.1029/2018JD029692

Donohoe A, Marshall J, Ferreira D, Mcgee D (2013) The relationship between ITCZ location and cross-equatorial atmospheric heat transport: from the seasonal cycle to the Last Glacial Maximum. J Clim 26:3597–3618

Donohoe A, Marshall J, Ferreira D, Armour K, McGee D (2014) The interannual variability of tropical precipitation and interhemispheric energy transport. J Clim 27:3377–3392

Gu G, Adler RF, Sobel AH (2005) The eastern Pacific ITCZ during the boreal spring. J Atmos Sci 62:1157–1174

Huffman GJ et al (1997) The global precipitation climatology project (GPCP) combined precipitation dataset. Bull Am Meteorol Soc 78:5–20

Kalnay E et al (1996) The NCEP/NCAR 40-year reanalysis project. Bull Am Meteorol Soc 77:437–472

Kang SM, Held IM, Frierson DM, Zhao M (2008) The response of the ITCZ to extratropical thermal forcing: Idealized slab-ocean experiments with a GCM. J Clim 21:3521–3532

Kang SM, Frierson DM, Held IM (2009) The tropical response to extratropical thermal forcing in an idealized GCM: the importance of radiative feedbacks and convective parameterization. J Atmos Sci 66:2812–2827

Li Y, Li JP, Feng J (2012) A teleconnection between the reduction of rainfall in southwest Western Australia and North China. J Clim 25:8444–8461

Li JP, Sun C, Jin FF (2013) NAO implicated as a predictor of Northern Hemisphere mean temperature multidecadal variability. Geophys Res Lett 40:5497–5502. https://doi.org/10.1002/2013GL057877

Liebmann B, Smith CA (1996) Description of a complete (interpolated) outgoing longwave radiation dataset. Bull Am Meteorol Soc 77:1275–1277

Liu Z, Ostrenga D, Teng W, Kempler S (2012) Tropical Rainfall Measuring Mission (TRMM) precipitation data and services for research and applications. Bull Am Meteorol Soc 93:1317–1325. https://doi.org/10.1175/BAMS-D-11-00152.1

McPhaden MJ, Zebiak SE, Glantz MH (2006) ENSO as an integrating concept in earth science. Science 314:1740–1745

Mechem D (2013) An introduction to dynamic meteorology. Bull Am Meteorol Soc 94:1917–1920

Mo KC, Higgins RW (1998) The Pacific-South American modes and tropical convection during the Southern Hemisphere winter. Mon Weather Rev 126(6):1581–1596

Pausata FS, Camargo SJ (2019) Tropical cyclone activity affected by volcanically induced ITCZ shifts. Proc Natl Acad Sci 116:7732–7737

Qin J, Zhou L, Ding R, Li J (2018) Influence of South Pacific quadrapole on austral winter precipitation over the SPCZ. Environ Res Lett. https://doi.org/10.1088/1748-9326/aadd84

Rayner N et al (2003) Global analyses of sea surface temperature, sea ice, and night marine air temperature since the late nineteenth century. J Geophys Res. https://doi.org/10.1029/2002jd002670

Saji N, Goswami B, Vinayachandran P, Yamagata T (1999) A dipole mode in the tropical Indian Ocean. Nature 401:360

Stuecker MF et al (2017) Revisiting ENSO/Indian Ocean dipole phase relationships. Geophys Res Lett 44:2481–2492

Trenberth KE (1976) Spatial and temporal variations of the Southern Oscillation. Q J R Meteorol Soc 102:639–653

Trenberth KE, Stepaniak DP (2000) Indices of El Niño evolution. J Clim 14:1697–1701. https://doi.org/10.1175/1520-0442(2001)014%3c1697:LIOENO%3e2.0.CO;2

Walker GT, Bliss EW (1932) World weather V. Mem R Meteorol Soc 4:53–84

Xie P, Arkin PA (1997) Global precipitation: a 17-year monthly analysis based on gauge observations, satellite estimates, and numerical model outputs. Bull Am Meteorol Soc 78:2539–2558

Xie SP, Philander SGH (1994) A coupled ocean–atmosphere model of relevance to the ITCZ in the eastern Pacific. Tellus Ser A Dyn Meteorol Oceanol 46:340–350

Zhan R, Wang Y, Lei X (2011) Contributions of ENSO and East Indian Ocean SSTA to the interannual variability of northwest Pacific tropical cyclone frequency. J Clim 24:509–521. https://doi.org/10.1175/2010JCLI3808.1

Zhang R, Delworth TL (2005) Simulated tropical response to a substantial weakening of the Atlantic thermohaline circulation. J Clim 18:1853–1860

Zhou X, Wang W, Ding R, Li J, Hou Z, Xie W (2019) An investigation of the differences between the North American Dipole and North Atlantic Oscillation. Atmosphere. https://doi.org/10.3390/atmos10020058